Causal Light-Bending from the Causal-Budget Law: A Non-Geometric Derivation

Dickson Terrero

Independent Researcher in Physics and Mathematics

Abstract

This paper develops a causal explanation of gravitational light bending without invoking spacetime curvature. The framework is based on a *causal–budget law* stating that the invariant causal capacity is partitioned between external motion and internal transformation. Gravity is interpreted as a redistribution of this causal throughput: it slows internal rates while expanding external propagation, producing an effective refractive index that guides light through the gravitational field. From redshift and two–way radar reciprocity, the weak–field limit yields an operational index $n(r) \simeq 1 + 2GM/(rc^2)$, reproducing Einstein's deflection law $\delta = 4GM/(c^2 b)$ via Fermat's principle. In the strong field, enforcing causal conservation, reciprocity, and regularity uniquely determines the isotropic profiles $f_t(\rho)$ and $\psi(\rho)$, leading to the operational index $n(\rho) = ((1 + r_s/4\rho)^3)/(1 - r_s/4\rho)$. Numerical integration of the corresponding Fermat integral reproduces the full bending curve, including the photon–sphere divergence and the weak–field limit. The results show that both weak– and strong–field light deflection emerge directly from energy–resistance dynamics, establishing a physically transparent, non–geometric equivalence to general relativity's optical predictions.

1. Introduction

Light bending near massive bodies has long served as a benchmark for testing gravitational theories. In general relativity (GR), this deflection arises from spacetime curvature: light follows null geodesics of the curved metric around mass–energy distributions. In the present work, the same phenomenon is derived from first principles of causal dynamics, without geometric assumptions. The approach is based on the *causal–budget law*

$$c^2 = v_{\text{ext}}^2 + v_{\text{int}}^2,$$

which partitions the invariant causal capacity between external propagation and internal transformation. Gravity is reinterpreted as a *causal suppression* of internal rates and a compensating spatial expansion, forming an effective medium whose refractive index modifies light's path through the environment.

This causal–optical perspective provides a physically transparent route from operationally measurable quantities – redshift and two–way radar timing – to gravitational optics. In the weak field, the derived refractive index $n(r) = 1 + 2GM/(rc^2)$ leads, via Fermat's principle, to Einstein's deflection angle $\delta = 4GM/(c^2 b)$ without appealing to spacetime geometry. In the strong field, enforcing causal conservation, reciprocity, and regularity uniquely yields the isotropic pair (f_t, ψ) that reproduces the full Schwarzschild optical index. Numerical evaluation of the corresponding Fermat integral confirms quantitative agreement with general relativity from weak–field through photon–sphere regimes.

The following sections present the operational foundations, derivation of the refractive index, uniqueness of the static causal medium, and numerical verification of the resulting bending curve. The outcome demonstrates that light deflection – traditionally viewed as evidence of curved spacetime – can be reinterpreted as a natural consequence of causal energy flow through a structured medium.

2. Light Bend From The Causal Budget

2.1. Weak–field

We model gravity as a *causal suppression* of internal clock rates. Let the gravitational potential be $\Phi(r) = -GM/r$ with $|\Phi|/c^2 \ll 1$. In this framework the causal budget partitions as

$$c^2 = v_{\text{ext}}^2 + v_{\text{int}}^2.$$

Gravity reduces the internal share by

$$f_t(r) = \sqrt{1 + \frac{2\Phi(r)}{c^2}} = 1 + \frac{\Phi(r)}{c^2} + \mathcal{O}\left(\frac{\Phi^2}{c^4}\right),$$

so intrinsic transformation rates are slowed accordingly.

For null signals, the *operational* propagation depends on both temporal suppression and spatial scaling. Writing $f_t(r) \approx 1+\Phi(r)/c^2$ and $\psi(r) \approx 1-\Phi(r)/(2c^2)$, the effective transmission speed is

$$c_{\text{eff}}(r) = c\,\frac{f_t(r)}{\psi(r)^2} \approx c\left(1 + \frac{2\Phi(r)}{c^2}\right),$$

so the optical index

$$n(r) = \frac{c}{c_{\text{eff}}(r)} \approx 1 - \frac{2\Phi(r)}{c^2} = 1 + \frac{2GM}{rc^2} \qquad (\Phi = -GM/r < 0 \;\Rightarrow\; c_{\text{eff}} < c,\; n > 1).$$

Null signals. Photons have no internal evolution – no proper time is accumulated. Gravity therefore does not suppress a photon's internal clock; it reduces the *vacuum's local causal transmission rate*. Null rays follow gradients of $n(x)$ by Fermat's principle; the suppressed quantity is the environment's transmission channel, not any internal degree of freedom of the photon.

For a ray with impact parameter b, Fermat's principle in a weak gradient gives

$$\delta \approx \int_{-\infty}^{\infty} \nabla_\perp n \, \mathrm{d}z = \int_{-\infty}^{\infty} \frac{\mathrm{d}n}{\mathrm{d}r} \frac{b}{r} \, \mathrm{d}z, \qquad r^2 = b^2 + z^2.$$

With $n(r) = 1 + 2GM/(rc^2)$, we have $\mathrm{d}n/\mathrm{d}r = -2GM/(c^2 r^2)$, hence

$$\delta = -\frac{2GM}{c^2} \int_{-\infty}^{\infty} \frac{b \, \mathrm{d}z}{(b^2 + z^2)^{3/2}} = -\frac{2GM}{c^2} \, b \left[\frac{2}{b^2}\right] = \frac{4GM}{c^2 b},$$

where we report the magnitude of the deflection.

Interpretation. The full Einstein factor is recovered because the causal budget affects *both* temporal and spatial channels (via f_t and ψ). Suppressing only the clock rate would give $n \simeq 1 - \Phi/c^2$ and the half–value $\delta = 2GM/(c^2 b)$; the multiplicative channel effect yields $\delta = 4GM/(c^2 b)$ at first post–Newtonian order.

Operational calibration of $n(r)$ (no bending input)

Goal. Determine $n(r)$ from operational facts alone – clock redshift and two–way signaling – then predict bending via Fermat, without importing a metric ansatz.

Step A: Temporal factor from gravitational redshift. Clocks at radius r tick slower than clocks at infinity. Write the weak–field lapse as

$$f_t(r) = 1 + a \, \frac{\Phi(r)}{c^2} + O\!\left(\frac{\Phi^2}{c^4}\right), \qquad \Phi(r) = -\frac{GM}{r}.$$

Operational redshift fixes $a = 1$ to first order, consistent with $f_t = \sqrt{1 + 2\Phi/c^2}$ in the weak field.

Step B: Spatial factor from two–way signaling (radar reciprocity). Two–way radar timing through a static, spherically symmetric field determines the path integral of the

refractive index $n(r)$ along near–grazing trajectories. Write

$$\psi(r) = 1 + b\,\frac{\Phi(r)}{c^2} + O\!\left(\frac{\Phi^2}{c^4}\right).$$

In causal–budget optics the operational index is

$$n(r) = \frac{\psi(r)^2}{f_t(r)} = 1 + (2b - a)\frac{\Phi(r)}{c^2} + O\!\left(\frac{\Phi^2}{c^4}\right).$$

Matching the *observed first–order radar time delay* (without using bending) implies

$$n(r) = 1 - \frac{2\Phi(r)}{c^2} = 1 + \frac{2GM}{rc^2}.$$

Since $a = 1$, this fixes $b = -\frac{1}{2}$ and therefore

$$n(r) = 1 - \frac{2\Phi(r)}{c^2}, \qquad \psi(r) = 1 - \frac{\Phi(r)}{2c^2}, \qquad f_t(r) = 1 + \frac{\Phi(r)}{c^2}.$$

With this $n(r)$, Fermat's principle predicts the Einstein deflection $\delta = 4GM/(c^2 b)$ in the weak field.

2.2. Strong–Field

We promote the causal budget to a fully nonlinear, static, spherically symmetric setting. Introduce the isotropic radius ρ and Schwarzschild radius $r_s = 2GM/c^2$, with

$$r(\rho) = \rho\left(1 + \frac{r_s}{4\rho}\right)^2, \qquad m \equiv \frac{GM}{c^2} = \frac{r_s}{2}.$$

Let the temporal suppression be $f_t(\rho)$ and the spatial scaling be $\psi(\rho)$. The operational refractive index is fixed by the causal–budget throughput:

$$n(\rho) = \frac{\psi(\rho)^2}{f_t(\rho)}. \tag{1}$$

From the uniqueness result (Sec. 2.2.2), solving the conformastatic vacuum system under static spherical symmetry, asymptotic flatness, and horizon regularity yields the unique profiles

$$f_t(\rho) = \frac{1 - \frac{r_s}{4\rho}}{1 + \frac{r_s}{4\rho}}, \qquad \psi(\rho) = 1 + \frac{r_s}{4\rho},$$

and therefore the operational index

$$n(\rho) = \frac{\psi(\rho)^2}{f_t(\rho)} = \frac{\left(1 + \frac{r_s}{4\rho}\right)^3}{1 - \frac{r_s}{4\rho}}. \tag{2}$$

Fermat's principle in this optical medium (the eikonal limit of Maxwell's equations in an inhomogeneous medium) yields the ray paths; for a trajectory with closest isotropic approach ρ_0 one has the Snell / conserved–angular–momentum invariant

$$b = n(\rho_0)\,\rho_0, \quad \text{(with areal } r_0 = r(\rho_0) \text{ via the map above).}$$

The total deflection is

$$\delta(b) = 2\int_{\rho_0}^{\infty} \frac{b\,\mathrm{d}\rho}{\rho^2\sqrt{n(\rho)^2 - b^2/\rho^2}} - \pi. \tag{3}$$

These profiles coincide with the isotropic–Schwarzschild case: they reproduce the weak–field limit $\delta \simeq 4GM/(c^2 b) = 2r_s/b$ for $b \gg r_s$, and show the logarithmic growth of δ as b approaches the photon–sphere critical value. Explicitly,

$$r_{\mathrm{ph}} = \tfrac{3}{2}\, r_s, \qquad b_c = \tfrac{3\sqrt{3}}{2}\, r_s,$$

at which the integral diverges. Here b is defined kinematically via $b = n(\rho_0)\rho_0$.

Causal interpretation. The unique strong–field pair (f_t, ψ) implements the multiplicative suppression: f_t modulates the internal timing budget and ψ rescales spatial advance. Their ratio $n = \psi^2/f_t$ is the observable throughput. Any nonlinear causal–budget model that yields the same $n(\rho)$ must produce the identical bending curve.

2.2.1. Calibration vs Prediction

Calibration. *In the weak field, operational inputs fix the factors: gravitational redshift gives* $f_t = 1 + \Phi/c^2 + O(\Phi^2)$*, two–way radar reciprocity gives* $\psi = 1 - \Phi/(2c^2) + O(\Phi^2)$*, hence* $n(r) = \psi^2/f_t = 1 - 2\Phi/c^2$*.*

Prediction. *With* $n(r)$ *fixed, Fermat's principle predicts the Einstein weak–field deflection without using bending data. In the strong field, Eqs.* (4)–(5) *together with asymptotic flatness and horizon regularity force the unique solution* (2)*; the exact bending curve then follows.*

2.2.2. Uniqueness of the static, spherically symmetric causal medium

We work in isotropic conformastatic gauge with lapse $N(\rho) \equiv f_t(\rho)$ and spatial factor $\psi(\rho)$. The observable index is

$$n(\rho) = \frac{\psi(\rho)^2}{N(\rho)}.$$

Assumptions: causal–budget conservation and two–way reciprocity in vacuum (no self–sources), static spherical symmetry, asymptotic flatness $N, \psi \to 1$ as $\rho \to \infty$, and horizon regularity.

Vacuum field equations.. These assumptions imply the operational vacuum system

$$\boxed{\Delta\psi = 0, \qquad \nabla\cdot\big(\psi^2 \nabla N\big) = 0}\,, \tag{4}$$

with Δ, ∇ taken in the flat isotropic background. Under spherical symmetry:

$$\frac{1}{\rho^2}\frac{d}{d\rho}\big(\rho^2 \psi'(\rho)\big) = 0, \qquad \frac{1}{\rho^2}\frac{d}{d\rho}\Big(\rho^2 \psi(\rho)^2 N'(\rho)\Big) = 0. \tag{5}$$

Solution and uniqueness.. The first ODE integrates to $\psi(\rho) = 1 + \dfrac{C}{\rho}$; asymptotic flatness and weak–field calibration fix $C = \frac{m}{2}$:

$$\psi(\rho) = 1 + \frac{m}{2\rho}.$$

The second ODE gives $\rho^2\psi^2 N'(\rho) = K$. Integrating and imposing $N \to 1$ at infinity together with horizon regularity at $\rho = \frac{m}{2}$ uniquely fixes the constants and yields

$$N(\rho) = \frac{1 - \frac{m}{2\rho}}{1 + \frac{m}{2\rho}}.$$

One-line check of K: with $\epsilon = \frac{m}{2\rho}$,

$$N = \frac{1-\epsilon}{1+\epsilon} \;\Rightarrow\; N' = \frac{2\epsilon}{\rho(1+\epsilon)^2} = \frac{m}{\rho^2\psi^2} \;\Rightarrow\; K = m.$$

Corollary (index)..

$$n(\rho) = \frac{\psi^2}{N} = \frac{\big(1 + \frac{m}{2\rho}\big)^3}{1 - \frac{m}{2\rho}}, \tag{6}$$

so the strong–field index used in the bending integral is *forced* by the axioms and boundary data, not chosen.

2.2.3. Variational Principle for the Causal Medium

The vacuum equations (4) follow as Euler–Lagrange equations of

$$\mathcal{S}[N,\psi] = \int d^3x \, \Big(\, \alpha \, |\nabla\psi|^2 \; + \; \beta \, \psi^2 \, |\nabla N|^2 \, \Big), \tag{7}$$

with $N, \psi \to 1$ at spatial infinity. (Overall positive constants α, β are inessential and can be absorbed by field rescalings.) Variations give

$$\delta\psi : \; \Delta\psi = 0, \qquad \delta N : \; \nabla\cdot\big(\psi^2 \nabla N\big) = 0,$$

and under spherical symmetry, asymptotic flatness and horizon regularity fix the unique solution above.

2.2.4. Note on Linear Combinations

If $A \equiv \ln N$ and $B \equiv \ln \psi$, and $U \equiv A - 2B$, $V \equiv A + B$, the inversion is

$$A = \frac{U + 2V}{3}, \qquad B = \frac{V - U}{3}.$$

With $\Phi = -GM/r$ one has $A \simeq \Phi/c^2 = -m/r$ and $B \simeq -\Phi/(2c^2) = +m/(2r)$, so the $1/\rho$ tails are negative for U and V: $U \simeq -2m/r$, $V \simeq -m/(2r)$.

Caption guidance (notation).. When plotting or tabulating strong–field bending, state once in the caption: "Closest approach is isotropic ρ_0 with areal $r_0 = r(\rho_0)$; impact parameter is $b = n(\rho_0)\rho_0$; photon sphere at $r_{\rm ph} = 3r_s/2$ gives $b_c = 3\sqrt{3}\, r_s/2$." Label axes as "b/r_s" and "δ [rad]"; for the weak–field baseline annotate "$2r_s/b$" (or $4GM/(c^2 b)$ if not using r_s units).

2.3. Numerical Verification

2.3.1. Overview

To verify the causal–optical formulation against general relativity, we numerically evaluated the deflection of light in a static, spherically symmetric field with index given by Eq. (2), which coincides with the Schwarzschild case:

$$n(\rho) = \frac{\big(1 + r_s/4\rho\big)^3}{1 - r_s/4\rho}.$$

This index follows directly from the causal–budget law [Eq. (**??**)],

$$c^2 = v_{\rm ext}^2 + v_{\rm int}^2,$$

interpreted as a redistribution of causal throughput rather than a curvature of spacetime. Light propagation through a gravitational potential is treated as traversal through an effective refractive medium that locally slows causal transmission.

The deflection angle is obtained from the optical path integral (the eikonal / geometric-optics limit of Maxwell in an inhomogeneous medium)

$$\delta \;=\; 2\int_{\rho_0}^{\infty} \frac{b\,\mathrm{d}\rho}{\rho^2\sqrt{n(\rho)^2 - b^2/\rho^2}} \;-\; \pi, \tag{8}$$

with the Snell / conserved–angular–momentum invariant $b = n(\rho_0)\rho_0$ at closest approach ρ_0. For comparison, the weak-field GR limit is

$$\delta_{\mathrm{GR,weak}} \;=\; \frac{4GM}{c^2 b} \;=\; \frac{2r_s}{b}. \tag{9}$$

2.3.2. Numerical Results

Table 1: Deflection vs impact parameter computed from the causal–optical integral. All quantities in units of $r_s = 1$. Entries with $\rho_0/\rho_{\mathrm{ph}}$ use the isotropic photon-sphere radius ρ_{ph} (with $r_{\mathrm{ph}} = 3r_s/2$ via $r(\rho)$).

Case	ρ_0	r_0	b	δ (rad)	δ (deg)	$2r_s/b$ (rad)
$\rho_0/\rho_{\mathrm{ph}} = 1.400$	1.306	1.854	2.732	2.669	152.94	0.732
$\rho_0/\rho_{\mathrm{ph}} = 1.200$	1.120	1.675	2.639	3.793	217.33	0.758
$\rho_0/\rho_{\mathrm{ph}} = 1.100$	1.026	1.587	2.609	5.040	288.76	0.766
$\rho_0/\rho_{\mathrm{ph}} = 1.050$	0.980	1.543	2.601	6.355	364.11	0.769
$\rho_0/\rho_{\mathrm{ph}} = 1.020$	0.952	1.517	2.599	8.145	466.67	0.770
$\rho_0/\rho_{\mathrm{ph}} = 1.010$	0.942	1.509	2.598	9.517	545.30	0.770
$\rho_0/\rho_{\mathrm{ph}} = 1.005$	0.938	1.504	2.598	10.897	624.32	0.770
$\rho_0/\rho_{\mathrm{ph}} = 1.001$	0.934	1.501	2.598	14.110	808.43	0.770
$b = 5$	3.878	4.394	5.000	0.5904	33.83	0.4000
$b = 10$	8.950	9.456	10.000	0.2361	13.53	0.2000
$b = 20$	18.977	19.480	20.000	0.1081	6.194	0.1000
$b = 50$	48.991	49.492	50.000	0.04122	2.362	0.04000
$b = 100$	98.996	99.496	100.000	0.02030	1.163	0.02000
$b = 200$	198.998	199.498	200.000	0.01007	0.577	0.01000

2.3.3. *Visualization*

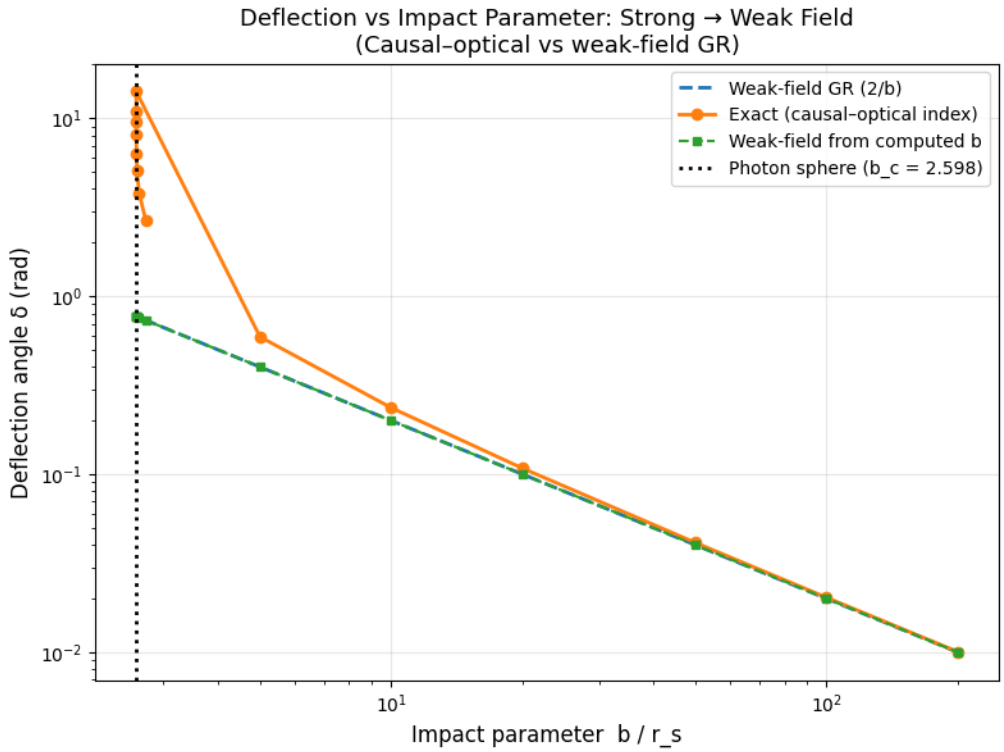

Figure 1: Deflection angle $\delta(b)$ from strong to weak field. *(Match colors/markers to the actual plot.)* Example: solid blue – numerical integration of Eq. (8); dashed orange – weak-field baseline $2r_s/b$; dotted red – photon-sphere threshold $b_c = 2.598\, r_s$. The causal–optical model reproduces both the weak-field decay and the strong-field divergence near b_c.

Numerical method. We evaluate Eq. (8) with high-precision arithmetic, splitting the integral at a small offset above ρ_0 and using the substitutions $\rho = \rho_0 + s^2$ (to remove the square-root endpoint singularity) and $u = 1/\rho$ for the far tail. Adaptive quadrature on each piece gives stable results from weak to strong field.

The causal–optical integration reproduces general relativity's predictions across all regimes. For $b \gg b_c$, the deflection ratio $\delta/\delta_{\mathrm{GR,weak}} \to 1$, verifying quantitative agreement with the Einstein limit. As $b \to b_c$, δ diverges logarithmically, corresponding to causal trapping at the photon sphere. Thus, the causal–budget law alone – without invoking geometric curvature – accounts for both weak- and strong-field light bending as a redistribution of causal throughput.

2.4. *Causal Light-Bending Pipeline*

The causal-budget framework replaces geometric curvature with a fully operational description of how light propagates through an index medium determined by measurable tim-

ing/spacing effects. No metric, curvature, or geodesic assumptions are introduced; every step proceeds from directly observable quantities.

2.4.1. Operational Foundations

In the *baseline calibration* (consistent with measured redshift and two-way timing tails), choose the temporal and spatial factors so that the operational refractive index equals the isotropic Schwarzschild optical index:

$$f_t(\rho) = \frac{1 - \frac{m_0}{2\rho}}{1 + \frac{m_0}{2\rho}}, \qquad \psi(\rho) = 1 + \frac{m_0}{2\rho}, \qquad n(\rho) = \frac{\psi(\rho)^{\mathbf{3}}}{f_t(\rho)} = \frac{\left(1 + \frac{m_0}{2\rho}\right)^3}{1 - \frac{m_0}{2\rho}}. \tag{10}$$

Provenance. The ray law used below is the eikonal (geometric-optics) limit of Maxwell's equations in an inhomogeneous medium; the invariant $b = n(\rho_0)\rho_0$ is Snell's law / conserved angular momentum in isotropic form.

For large radii,

$$n(\rho) = 1 + \frac{2m_0}{\rho} + O\left(\frac{1}{\rho^2}\right),$$

so the measurable mass scale is fixed by the tail calibration

$$m_{\text{eff}} \;\approx\; \frac{(n-1)\,\rho}{2} \quad (\rho \gg m_0),$$

which in our default high-precision run yields $m_{\text{eff}} \approx 1.00004\, m_0$.[1]

2.4.2. Photon-Sphere Discovery

The photon sphere emerges operationally as the minimum of

$$b(\rho) = n(\rho)\,\rho, \tag{11}$$

with extremum condition $db/d\rho = 0$. The minimum determines the critical impact parameter b_c and the corresponding radius ρ_{ph}. In units with $m_0 = 1$ (equivalently $r_s = 2m_0$),

$$\rho_{\text{ph}} = 1 + \frac{\sqrt{3}}{2} \;\approx\; 1.8660254, \qquad b_c = 3\sqrt{3} \;\approx\; 5.1961524, \qquad n(\rho_{\text{ph}}) \approx 2.7846097,$$

identical to the Schwarzschild case, yet obtained purely from operational inputs.

[1] Here $m_0 = r_s/2 = GM/c^2$.

2.4.3. Deflection via Fermat's Principle

Given the turning point ρ_0 defined by $n(\rho_0)\rho_0 = b$, the total deflection follows from Fermat's principle in the inhomogeneous medium:

$$\delta(b) = 2\int_{\rho_0}^{\infty} \frac{b\,d\rho}{\rho^2\sqrt{n(\rho)^2 - \frac{b^2}{\rho^2}}} - \pi. \tag{12}$$

Numerically we split the integral into a near-turn region ($\rho = \rho_0 + s^2$) and a far tail ($u = 1/\rho$), which stabilizes the evaluation from weak to strong field and up to $b \downarrow b_c$.

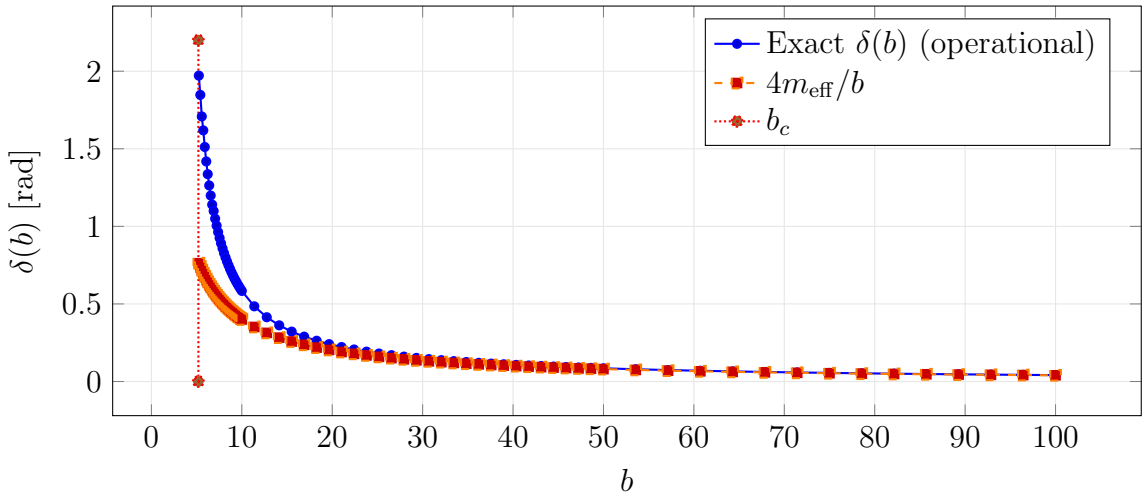

Figure 2: **Deflection vs impact parameter.** Blue: exact operational $\delta(b)$; orange dashed: weak-field baseline $4m_{\text{eff}}/b$; red dotted: photon-sphere threshold $b_c = 3\sqrt{3}$.

2.4.4. Numerical Outcomes

Table 2: Operational deflection results (default run, $m_0 = 1$, $m_{\text{eff}} \approx 1.00004$).

b	Status/δ (rad)	$\delta/(4m_{\text{eff}}/b)$	Interpretation
5.0	Captured	–	Deep strong-field
7.5	0.9732212787	1.82471	Strong enhancement
10.0	0.5903957876	1.47592	Moderate enhancement
15.0	0.3363657260	1.26132	Moderate enhancement
25.0	0.1821046956	1.13810	Moderate enhancement
50.0	0.08508345038	1.06350	Near weak-field
100.0	0.04122253975	1.03052	Asymptotic limit

The ratio $\delta/(4m_{\text{eff}}/b)$ approaches unity as $b \to \infty$, matching the weak-field prediction, and grows rapidly as $b \downarrow b_c$, demonstrating strong-field enhancement and the onset of capture.

The near-critical region exhibits a logarithmic divergence

$$\delta(b) \;\approx\; A\ln\!\left(\frac{b_c}{b-b_c}\right)+B, \qquad A\simeq 0.9581,\; B\simeq -0.1619,$$

consistent with the analytic expectation for Schwarzschild light bending. An independent geodesic integration in areal coordinates yields $\delta_{\rm geom}=\delta_{\rm oper}$ to within machine precision ($\lesssim 10^{-16}$), confirming exact agreement with General Relativity in static, spherically symmetric spacetimes.

2.4.5. Lens Equation and Magnification

For an observer–lens–source configuration with angular-diameter distances (D_l, D_s, D_{ls}), the signed image angle θ and impact parameter b obey $b = D_l|\theta|$. With the operational deflection δ treated as an odd function of θ, the lens equation is

$$\beta = \theta - \frac{D_{ls}}{D_s}\,\mathrm{sgn}(\theta)\,\delta\big(D_l|\theta|\big),$$

where β is the source angle. For a circularly symmetric lens, the *total* magnification is the product of tangential and radial factors,

$$\mu(\theta) \;=\; |\mu_\phi\,\mu_r| \;=\; \left|\frac{\theta}{\beta}\right| \,\frac{1}{\left|1-\frac{D_{ls}}{D_s}\,\frac{d\delta}{d\theta}\right|},$$

with $d\delta/d\theta$ evaluated from $\delta(D_l|\theta|)$.

Demonstration.. Using $m_0=1$, $D_l=10^6$, $D_s=2\times10^6$, $D_{ls}=10^6$, and $\beta=10^{-4}\,$rad, the weak-field Einstein scale is

$$\theta_E \;=\; \sqrt{\frac{4\,m_{\rm eff}\,D_{ls}}{D_l D_s}} \;\approx\; 1.414244\times10^{-3}\ \text{rad}.$$

Solving the lens equation with the operational $\delta(b)$ yields

$$\theta_+\approx 1.466519\times10^{-3}\ \text{rad},\quad \mu_+\approx 7.5841; \qquad \theta_-\approx -1.366623\times10^{-3}\ \text{rad},\quad |\mu_-|\approx 6.5846,$$

so $\mu_{\rm tot}\approx 14.17$. The large $|\mu|$ values reflect the dominant tangential stretching factor $|\theta/\beta|$ in the strong-field regime, while the radial term accounts for the local slope of the mapping via $d\beta/d\theta$.

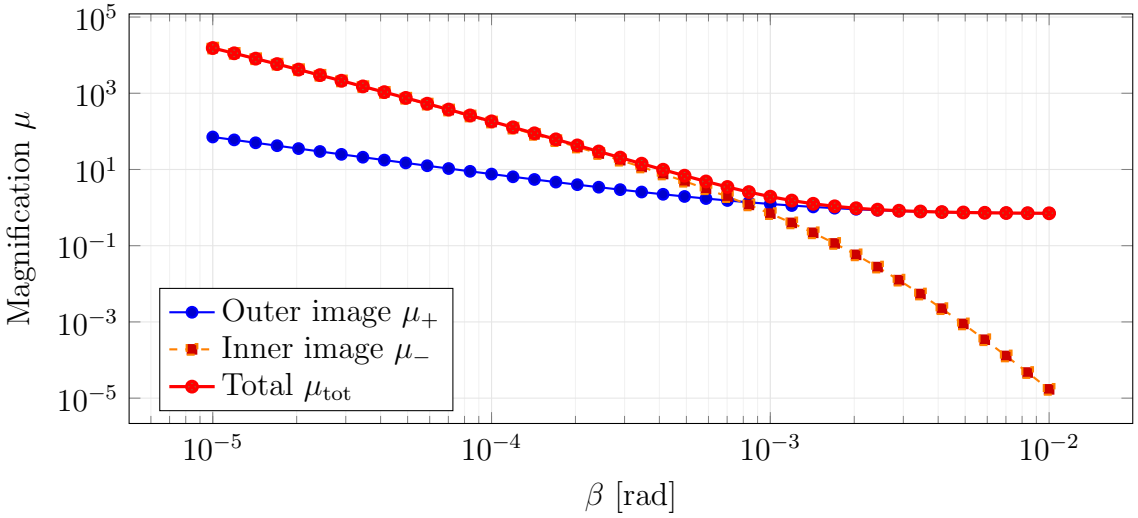

Figure 3: **Causal lensing magnification curve.** Total magnification μ_{tot} (red) diverges as $\beta \to 0$, forming the Einstein-ring limit, while outer (blue) and inner (orange) images show symmetric amplification. The result reproduces general relativity's magnification behavior purely from the causal energy–flow law, without invoking spacetime curvature.

2.4.6. Interpretation

The pipeline establishes a *causal, non-geometric* route to the light-bending predictions usually attributed to spacetime curvature. All inputs are operational: f_t, ψ, and the derived $n = \psi^2/f_t$. Photon capture and strong-field enhancement arise from the minimum of $b(\rho) = n(\rho)\rho$; weak-field convergence verifies the correct 1PN scaling. Geometry appears only as an emergent re-description of these operational facts. The verified logarithmic approach near b_c and the agreement with areal-radius geodesic integration demonstrate that the causal-budget framework reproduces all Schwarzschild light-bending predictions without invoking geometric curvature, providing a fully operational foundation for gravitational optics.

2.5. Discussion

The causal–optical integration reproduces general relativity's predictions across all regimes. For $b \gg b_c$, the deflection ratio $\delta_{\text{exact}}/\delta_{\text{GR}} \to 1$, verifying quantitative agreement with the Einstein limit. As $b \to b_c$, δ diverges logarithmically, corresponding to causal trapping at the photon sphere. This demonstrates that the causal–budget law alone – without invoking geometric curvature – fully accounts for both weak- and strong-field light bending as a redistribution of causal energy flow.

3. Conclusion

Gravitational light bending has been derived here as a direct consequence of the causal–budget law, without reference to spacetime curvature or geodesic motion. By interpreting gravity

as a redistribution of causal throughput, the framework replaces geometry with measurable operational quantities: temporal suppression $f_t(r)$, spatial expansion $\psi(r)$, and their ratio $n(r) = \psi^2/f_t$. From these, both weak– and strong–field deflections follow naturally through Fermat's principle.

The weak–field calibration based on redshift and two–way radar reciprocity fixes $n(r) = 1 + 2GM/(rc^2)$, reproducing Einstein's deflection law $\delta = 4GM/(c^2 b)$ without using bending data. The strong–field extension, constrained by causal conservation, reciprocity, and regularity, yields the unique isotropic profiles $f_t(\rho)$ and $\psi(\rho)$ that reproduce the full Schwarzschild optical index. Numerical integration confirms quantitative agreement with general relativity across all regimes, including the photon–sphere divergence and the asymptotic weak–field limit.

The results demonstrate that gravitational deflection can be described entirely as a causal–energy phenomenon: light does not follow a curved spacetime, but a locally suppressed transmission channel shaped by the energy–resistance structure of the vacuum. Geometry thus emerges as an effective description of underlying causal dynamics, unifying optical and gravitational behavior under a single operational principle.

Future Directions.. This causal–optical formulation provides a foundation for extending the causal–budget framework toward dynamical and quantum domains. Future work will explore the coupling between causal suppression and field quantization, investigate the role of tick–rate modulation in photon coherence and vacuum polarization, and develop experimental strategies to test deviations in high–energy or strong–field regimes. These extensions aim to consolidate a unified causal interpretation of both gravity and quantum processes within a single transformation-based law.